A luminescent nanocrystal stress gauge

Charina L. Choi[a,b,1], Kristie J. Koski[a,b,1,], Andrew C. K. Olson[a,b], A. Paul Alivisatos[a,b,2]

[a]Material Sciences Division, Lawrence Berkeley National Laboratory, Berkeley, CA 94720

[b]Department of Chemistry, University of California, Berkeley, CA 94720

[1]These authors contributed equally to this work.

[2]To whom correspondence may be addressed. Lawrence Berkeley National Lab, 1 Cyclotron Road Mail Stop 50A-4119, Berkeley, CA 94720

telephone: 510-486-5111

fax: 510-486-6720

e-mail: APAlivisatos@lbl.gov

Abstract.

Microscale mechanical forces can determine important outcomes ranging from the site of material fracture to stem cell fate. However, local stresses in a vast majority of systems cannot be measured due to the limitations of current techniques. In this work, we present the design and implementation of the CdSe/CdS core/shell tetrapod nanocrystal, a local stress sensor with bright luminescence readout. We calibrate the tetrapod luminescence response to stress, and use the luminescence signal to report the spatial distribution of local stresses in single polyester fibers under uniaxial strain. The bright stress-dependent emission of the tetrapod, its nanoscale size, and its colloidal nature provide a unique tool that may be incorporated into a variety of micromechanical systems including materials and biological samples to quantify local stresses with high spatial resolution.

A luminescent nanocrystal stress gauge

\body

Local microscale stresses play a crucial role in inhomogeneous mechanical processes from cell motility to material failure. Stress ($\sigma_{a,b} = F_a/A_b$) is a tensor quantity with components in the directions of applied and effected perturbations, and is related linearly to strain ($\varepsilon_{\alpha,\beta} = \int dl_{\alpha,\beta}/l_{\alpha,\beta}$) for small strains in an elastic solid via the stiffness constants, following Hooke's Law. Contact-probe techniques that measure stiffness such as atomic force microscopy (1, 2), indentation testing (3), and optical coherence elastography (4), and non-contact techniques that measure stress such as micro-Raman spectroscopy (5), electron backscatter diffraction (6), and polymeric post arrays (7) have been used to quantify local mechanical behavior with high spatial resolution. However, these techniques remain limited to studies in specific material systems due to spectroscopic and geometric constraints. For example, although the mechanical behavior of cells can be indicative of significant aspects of their biology, including metastatic potential (8), the stresses exerted by cells in physiologic three-dimensional culture systems cannot currently be quantified. A luminescent nanocrystal probe, with its small size, bright and narrow emission, and colloidal processability is ideally suited to measure local stresses in a variety of systems without spectroscopic requirements from or excessive perturbations to the material of interest.

We present here the design and implementation of a luminescent nanocrystal stress gauge, the CdSe/CdS core/shell tetrapod. The tetrapod, with a CdSe quantum dot at its core, has the same advantages as its widely used quantum dot predecessor, including tunable quantum confinement and high fluorescence quantum yields (9). Four CdS arms protruding from the CdSe core confer a branched, three-dimensional structure on the tetrapod; these arms can act as dynamic levers to torque the CdSe core and alter its optical response. The tetrapod can be incorporated into many materials, yielding a local stress measurement through optical

fluorescence spectroscopy of the electronically confined CdSe core states. In this report, we calibrate the stress response of the tetrapod, and use this calibration to study spatially-resolved mechanical behavior in single polymer fibers. We expect that tetrapods can be used to probe local stresses in many other mechanical systems.

The tetrapod nanocrystal is a tetrahedrally symmetric particle consisting of a zinc-blende core with four epitaxially-attached wurtzite arms (10) (Fig. 1a). Atomic force microscopy studies on CdTe tetrapods demonstrated that nanonewton forces are capable of bending these lever arms (11). Furthermore, electronic level structure calculations on CdSe tetrapods predicted that force-induced arm bending, which causes a strain in the nanocrystal, results in a red-shift of the energy gap (12). CdSe/CdS core/shell tetrapods, with a CdSe core and CdS arms, have high fluorescence quantum yields up to 60% due to quasi-type I band alignment of the heterostructure (13-15), and therefore present an optimal design for optical readout of local stresses. Compression of CdSe/CdS tetrapods in a diamond anvil cell revealed differential photoluminescence behavior under hydrostatic and non-hydrostatic pressure environments (16). These results suggested that the tetrapod might be useful as a gauge capable of sensing and optically reporting environmental stresses.

Results and Discussion

To develop the tetrapods as a luminescent stress gauge, we first calibrated the fluorescence response of tetrapods to non-hydrostatic stress in a simple uniaxial geometry, and then used this response to report local stresses in synthetic polymer fibers. Tetrapods were incorporated into single polyester fibers with known stress-strain properties and the tetrapod fluorescence was monitored under increasing tensile strain. CdSe/CdS tetrapods (4.8 ± 1.2 nm arm diameter and 27.8 ± 3.5 nm arm length) in low concentrations are easily incorporated into the fiber without perturbing the mechanical properties by dropping a few microliters of dilute solution in

toluene onto the fiber (see Methods). The toluene quickly evaporates, and red fluorescence (Fig. 1b) shifted from that of tetrapods in solution (Fig. 2a) is exhibited at all focal planes within the fiber, indicating that tetrapods are dispersed throughout. Diffusion of tetrapod fluorescence along the fiber following solvent evaporation was not observed, suggesting that tetrapods are relatively immobilized, along with their surface ligands. The chemistry of these surface ligands could be used to control tetrapod-matrix interactions; in this work, however, the tetrapods are simply dispersed in the matrix with no molecular scale anchoring. Scanning electron microscopy (SEM) images of a fiber cross-section confirm that tetrapods are embedded and well-distributed within (Fig. 1c).

Single polyester fibers with embedded tetrapods were affixed at both ends and tetrapod fluorescence spectra were monitored at a fixed spot with increasing tensile strain (see Methods). A clear spectral red-shift is evident as a result of increasing fiber extension (Fig. 2a). This shift is detectable with a spectral resolution of 0.01 nm in our system. The slight shoulder at higher-energy in each trace (blue arrow), which matches the spectral peak of tetrapods in solution, is attributed to a fractional population of tetrapods on the surface of the fiber. Although the refractive indices of the fiber also change as the fiber is extended, this change is within ± 0.02 and not large enough to induce the shifts we observe (17). Similarly, the temperature change from tensile loading contributes a maximum fluorescence band-gap shift of about ± 0.02 nm (18-20), a comparatively minor effect. The initial fluorescence wavelength maximum as well as the magnitude of the red-shift varies both spatially along the fiber as well as among different fibers (Fig. 2b), consistent with previous observations of mechanical variation in microstructure within and among single fibers (21, 22). In fact, the branched nature of the tetrapod may enable it to sense and report relevant length scales of spatial and dynamic heterogeneity down to the dimension of a tetrapod arm diameter. The initial fluorescence spectrum is recovered upon fiber failure and matrix relaxation, suggesting that under these experimental conditions the tetrapod

deformation remains elastic, as expected from previous observations of fluorescence reversibility (16).

Applied stresses to the tetrapod from fiber strain directly affect the energy gap, and therefore we studied the change in peak photoluminescence energy as a function of the fiber extension (Fig. 2b). The linear elastic regime and onset of plasticity are readily identified in the photoluminescence behavior. The average of individual fibers is expected to reflect bulk behavior. The average fluorescence slope versus true strain in the elastic regime was correlated with the known average Young's modulus of 8.3 ± 1.9 GPa (22) in order to calibrate the stress gauge. We determined a fluorescence shift of -5.8 ± 1.2 meV/GPa (see Methods). This value is comparable to the theoretical prediction of -30.8 meV/GPa for single material CdSe tetrapods (12), especially considering that differences in the strain dependence should exist due to altered wavefunction localizations within the hetero- and single material structures (13-15), and that different sizes of tetrapods were considered in the two studies. Additionally, the measured response to uniaxial stress is about one-fourth the magnitude of the photoluminescence blue-shift response to hydrostatic pressure (16). The calibration error is due to uncertainty from the linear fit; measurement error due to the spectral resolution and peak-fitting uncertainty corresponds to a stress resolution of 0.003 GPa.

Conventional measurement of the true stress in a fiber requires accurate knowledge of the diameter change, which is difficult to measure in fibers of microscale diameter. The tetrapod stress gauge avoids this difficulty by responding directly to the local true stress. As a proof-of-principle demonstration we applied the polyester-derived calibration to find the Young's moduli (E) of two high performance fibers of known E: Nomex® (10 μm diameter), a stiffer fiber than polyester, and nylon (120 μm diameter), a more compliant fiber. We found E = 18.9 ± 3.0 GPa and 4.3 ± 1.3 GPa for Nomex® and nylon respectively, within the range of accepted values for

these materials (23, 24) (Fig. 2c). The reported error values represent the error in calculated modulus due to the linear fit (see Methods). The calculated E for Nomex® is slightly higher than the accepted value, likely because we typically focused on a kink band in these thin fibers to easily mark the location for repeated measurements. Two limiting behaviors of sensitivity to the Young's modulus of the host medium exist. If the tetrapod probe is stiffer than the host medium and will not be easily deformed, then stress is transferred to the probe. If the tetrapod probe is less stiff than the host medium, it will move with the medium, thus adopting the strain of the material. As a result the upper limit that the tetrapod can detect is the modulus of the tetrapod itself. Tensile experiments on single Spectra® fibers, E = 103 GPa, suggest a Young's modulus of 50 GPa. This is roughly the Young's modulus of bulk CdSe, suggesting that the sensitivity of this stress gauge is limited to materials with moduli less than 50 GPa. Although nanoparticles at higher concentrations can change the mechanical properties of a polymer matrix (25), the dilute amounts of tetrapods incorporated here did not significantly affect the mechanical behavior of these fibers as evidenced by an unchanged true strain to failure and unaffected site of failure (see Methods).

The luminescent tetrapod stress gauge enables the imaging of local stresses within a complex medium. The ability to study local mechanical behavior is critical to an understanding of a material's response to external perturbations; for example, polymer fibers do not respond homogeneously under tensile strain, and a local instability may ultimately become the site of fiber failure. Ediger and colleagues studied the local mobilities associated with plastic flow within a polymer glass below the glass transition temperature. Upon perturbation with a fixed stress above a low-stress threshold, they observed not only an increase in the polymer mobility, as predicted by the Eyring model, but also a subsequent increase in the homogeneity of local mobility rates. Further polymer creep and recovery, leading to a decrease in the polymer mobility, resulted in a re-spreading of the mobility rate distribution. They suggested that local

stresses would mirror this behavior, with greater stresses in slower regions enabling higher mobility (26). We used the tetrapods to spatially resolve the local stress profile of a semicrystalline polyester fiber under increasing tensile strain (Fig. 3). Tetrapods were incorporated along an 8 mm stretch of polyester fiber, and fluorescence spectra were collected at adjacent spots 400 μm in length, of similar spot size to that studied by Ediger et al., as the fiber was extended up to 22.5% (Fig. 3a, see Methods). The ensemble red-shift with increasing tensile strain is clearly seen in the data. In addition, we observe a stress distribution narrowing in the elastic regime, followed by a distribution widening (Fig. 3b). This result indicates that the stress first becomes more homogeneous with strain and then increases in heterogeneity, correlating well with the previous observations of local mobility.

The CdSe/CdS tetrapods studied here present an optimal size and shape for sensing stress. Tensile stretching experiments on single polyester fibers embedded with tetrapods of similar diameter but longer (42.8 ± 2.8) or shorter (15.1 ±1.7) arm lengths both exhibit reduced stress sensitivity (Fig. 4a). We hypothesize that while a longer tetrapod arm may increase the amount of torque on the CdSe core and thus the stress sensitivity, an arm that is too long should additionally buckle, reducing the stress sensitivity. The effects of torque sensitivity and buckling will be maximized and minimized, respectively, in an optimal tetrapod arm aspect ratio for stress sensing. In addition, the tetrapod morphology is unqiue to sensing anisotropic stresses. Similar polyester fiber tensile experiments using CdSe/CdS quantum dots and rods demonstrate that these nanoscale geometries cannot specifically detect anisotropic stresses (Fig. 4b). Quantum dots (7.0 ± 1.1 nm diameter) exhibited a blue-shift with increasing fiber strain, similar to their behavior under hydrostatic pressure (16). Quantum rods, which from different viewing axes appear similar to either the dots or the tetrapods, exhibited either a slight red- or blue-shift with increasing tensile strain, suggesting that local rod orientation relative to the fiber affects the response to strain. No average net shift was observed for these particles.

Due to its nanoscale size, three-dimensional branched geometry, bright luminescence signature, and colloidal processability, the tetrapod nanocrystal possesses the ability to report both spatially- and dynamically-resolved stresses in many mechanical systems. The high quantum yield of the tetrapod enables luminescence measurements down to the single particle scale (27). Utilizing dark-field or super-resolution microscopies, the stress profile within a material may ultimately be mapped with spatial resolution of a single tetrapod. Tetrapods may also be biofunctionalized for studies including local stress measurements within biological fibers and three-dimensional cell culture, a method complementary to the use of collagen contrast (28), bead fluorescence (29), and gold nanorod scattering (30, 31) for measurement of local mechanical strains in a matrix. In both the mechanobiology and single tetrapod studies, the stress symmetry and its orientation relative to the tetrapods may be more complex than simple uniaxial or hydrostatic deformations on a tetrapod ensemble, and a deeper understanding of the optoelectronic response to other stress states is essential. Current efforts toward these goals are underway. Future synthetic work will allow creation of tetrapods of different sizes sensitive to stresses of a variety of magnitudes, and tetrapods of different compositions with alternate optical band gaps and particle stiffness, expanding the range of material systems and processes that may be probed.

Methods

Synthesis of CdSe/CdS dots, rods, and tetrapods. CdSe/CdS dots were synthesized following Li et al. (32), and CdSe/CdS rods and tetrapods were synthesized following Talapin et al. (14).

Polymer fibers. Transparent polyester thread (Coats & Clark, 90 μm diameter), transparent nylon thread (Sew Gude, 120 μm diameter), single fibers removed from spun Nomex® (The

Thread Exchange, 10 μm diameter), and Spectra® thread (Gudebrod GX2, 130 den, 20 μm diameter) were used for these experiments.

Incorporation of tetrapods into single polymer fibers. 1-5 μL of CdSe/CdS nanocrystals (9.1 x 10^{-10} M in toluene) were dropped onto a 3 mm (single spot studies) or 1 cm (stress profile studies) length of fiber, with a total of about 10^{-15} mol nanocrystals added to the fiber spot. The toluene quickly evaporates, resulting in single polymer fibers with nanocrystals embedded within (Fig. 1b and 1c). In most experiments, a kink band or a transverse band inherent to the fiber, or a black permanent mark on the fiber, was used as a reference mark to ensure that fluorescence spectra were collected at the same spot with subsequent fiber extension.

Tensile fluorescence experiments. Each end of a single polymer fiber was secured by winding under a washer and screw to a platform on a micrometer stage, with about 2 cm initial distance between the screws. One platform was fixed in position while the other could be controlled using the micrometer stage screw. The distance between the two screws was calibrated with the micrometer screw reading using digital calipers. A micrometer stage controller was used to extend the fiber.

The nanocrystal fluorescence was excited with a 488 nm Ar^+ laser (Lexel Laser, Inc., 95) with 2 mW power and 400 μm spot size at the sample. Brightfield and fluorescence images were taken with a digital microscope camera (Paxcam 2+). The fluorescence spectra were monitored using a home-built inverted fluorescence microscope with a spectrometer (Acton Research Corporation, SpectraPro-3001) and CCD detector (Princeton Instruments, Model 7509-0001). Exposure times of about 0.1s were used to collect spectra.

For stress profile experiments, fluorescence was monitored similarly, with a reference mark on the polyester fiber used as the initial point for each subsequent fiber extension. Tetrapods were embedded over an 8 mm length of single polyester fiber. A fluorescence

spectrum was taken at 20 adjacent spots of 400 μm spot size at 0% fiber extension. Subsequent spectra were taken at 2.5%, 5%, 7.5%, 10%, 12.5%, 15%, 17.5%, 20%, and 22.5% extension, with an increasing number of spots up to 26 adjacent spots taken at 22.5% extension due to increased fiber length. The length of fiber exhibiting tetrapod fluorescence increased as the fiber was extended and spectra were collected over this entirety, with the first spectrum always taken at the reference position (Fig. 3a).

Stress gauge calibration and Young's modulus measurements. The tetrapod fluorescence emission-maximum in polyester fiber was averaged from 17 individual experiments and plotted versus the true strain (ε_t = ln [1+0.01*(%extension)]). The slope in the elastic region was determined using a linear least squares fit on the first five mean data points, representing data from ε_t = 0 to 0.022 (0% to 2.2% fiber extension), with r^2 = 0.99. The error reported represents the 95% confidence interval for the fit in slope. The tetrapod fluorescence red-shift as a function of stress was then calculated using the reported average Young's modulus of 8.3 GPa for this polyester fiber (22).

To calculate the Young's modulus in single Nomex® and nylon fibers using the polyester-derived calibration, we determined the slope of the average emission-maximum versus strain for these fibers as described for polyester above. Four Nomex® experiments and five nylon experiments were used to obtain the average values. The slope in the elastic region for Nomex® was determined using the first 12 data points, representing data from ε_t = 0 to 0.017 (0% to 1.7% fiber extension), with r^2 = 0.95. The slope in the elastic region for nylon was determined using the first 10 data points, representing data from ε_t = 0 to 0.049 (0% to 4.9% fiber extension), with r^2 = 0.88. The error in measured Young's modulus for both Nomex® and nylon represents the 95% confidence interval for the fit in slope. For all three fibers, a maximum r^2 and subsequent difference in slope were used to determine the elastic limit. The data points

used to calculate Young's modulus are within the range of extensions considered in typical mechanical Young's modulus measurements for the respective material fibers.

Mechanical behavior of single fibers with and without embedded tetrapods. The percent extension to failure was measured for single fibers with and without tetrapods embedded, reported as [with tetrapods; without tetrapods]: polyester: [21.2 ± 3.7; 23.4 ±2.2], Nomex®: [16.0 ± 12.1; 30.9 ±10.4]; nylon: [15.4 ± 1.5, 16.9 ± 1.8]. The results with and without tetrapods are within error. The difference in percent extensions to failure and large standard deviations for Nomex® may be due to the thin diameter of Nomex, which makes fiber manipulation difficult. The location of fiber failure for all three fibers was unaffected by the addition of tetrapods.

Acknowledgements

We greatly thank Jessy L. Baker for scanning electron microscopy images of our sample and helpful discussions. We also thank Bryce Sadtler for helping to implement the fluorescence microscope, James H. Nelson for CdSe/CdS rod samples, Lynn Browne and Walter Webb for mechanical specifications of the polyester fiber sample, and Jonathan Chou and Young-wook Jun for helpful discussions and careful reading of the manuscript. Research was supported by the U.S. Department of Energy, Office of Basic Energy Sciences, Division of Materials Sciences and Engineering under Contract No. DE-AC02-05CH11231 [K.J.K., A.C.K.O., A.P.A., and the design and development of the stress gauge for non-biological applications] and the NIH Roadmap Initiative in Nanomedicine through Nanomedicine Development Center award PN2EY016546 [C.L.C. and the development of the stress gauge for biological applications].

Author Contributions

C.L.C., K.J.K., and A.P.A. designed the experiments and wrote the paper. C.L.C. and K.J.K. performed the experiments and analyzed the results. A.C.K.O. synthesized the CdSe/CdS tetrapods with longer and shorter arms.

Competing Financial Interests statement

The authors declare no competing financial interests. Correspondence and requests for materials should be addressed to A.P.A.

References

1. Rabe U, Janser K, Arnold W (1996) Vibrations of free and surface-coupled atomic force microscope cantilevers: Theory and experiment. *Review of Scientific Instruments* 67:3281-3293.
2. Yamanaka K, Nakano S (1996) Ultrasonic atomic force microscope with overtone excitation of cantilever. *Jpn. J. Appl. Phys.* 35:3787-3792.
3. Oliver WC, Pharr GM (2004) Measurement of hardness and elastic modulus by instrumented indentation: Advances in understanding and refinements to methodology. *J. Mater. Res.* 19:3-20.
4. Liang X, Oldenburg AL, Crecea V, Chaney EJ, Boppart SA (2008) Optical micro-scale mapping of dynamic biomechanical tissue properties. *Opt. Express* 16:11052-11065.
5. De Wolf I (1996) Micro-Raman spectroscpy to study local mechanical stress in silicon integrated circuits. *Semicond. Sci. Technol.* 11:139-154.
6. Vaudin MD, Gerbig YB, Stranick SJ, Cook RF (2008) Comparison of nanoscale measurements of strain and stress using electron back scattered diffraction and confocal Raman microscopy. *Appl. Phys. Lett.* 93:193116.
7. Tan JL et al. (2003) Cells lying on a bed of microneedles: an approach to isolate mechanical force. *Proc. Natl. Acad. Sci. USA* 100:1484-1489.
8. Butcher DT, Alliston T, Weaver VM (2009) A tense situation: forcing tumour progression. *Nat Rev Cancer* 9:108-122.
9. Alivisatos AP (1996) Semiconductor clusters, nanocrystals, and quantum dots. *Science* 271:933-937.
10. Manna L, Milliron DJ, Meisel A, Scher EC, Alivisatos AP (2003) Controlled growth of tetrapod-branched inorganic nanocrystals. *Nat. Mater.* 2:382-385.
11. Fang L et al. (2007) Mechanical and electrical properties of CdTe tetrapods studied by atomic force microscopy. *J. Chem. Phys.* 127:184704.

12. Schrier J, Lee B, Wang LW (2008) Mechanical and electronic-structure properties of compressed CdSe tetrapod nanocrystals. *J. Nanosci. Nanotechnol.* 8:1994-1998.

13. Müller J et al. (2005) Wave function engineering in elongated semiconductor nanocrystals with heterogeneous carrier confinement. *Nano Lett.* 5:2044-2049.

14. Talapin DV et al. (2007) Seeded growth of highly luminescent CdSe/CdS nanoheterostructures with rod and tetrapod morphologies. *Nano Lett.* 7:2951-2959.

15. Steiner D et al. (2008) Determination of band offsets in heterostructured colloidal nanorods using scanning tunneling spectroscopy. *Nano Lett.* 9:2954-2958.

16. Choi CL, Koski KJ, Sivasankar S, Alivisatos AP (2009) Strain-Dependent Photoluminescence Behavior of CdSe/CdS Nanocrystals with Spherical, Linear, and Branched Topologies. *Nano Lett.* 9:3544-3549.

17. Venkataprasad Bhat S, Govindaraj A, Rao CNR (2006) Tuning the emission bands of nanophosphors through the refractive index of the medium. *Chem. Phys. Lett.* 422:323-327.

18. Lindhagen JE, Berglund LA (1997) Temperature changes in polymer composites during tensile loading. *J. Mater. Sci.* 32:4071-4076.

19. Sih GC, Tzou DY, Michopoulos JG (1987) Secondary temperature fluctuation in cracked 1020 steel specimen loaded monotonically. *Theor. and Appl. Fract. Mech.* 7:79-87.

20. Li S, Zhang K, Yang JM, Lin L, Yang H (2007) Single quantum dots as local temperature markers. *Nano Lett.* 7:3102-3105.

21. Hosemann R (1962) Crystallinity in high polymers, especially fibres. *Polymer* 3:349-392.

22. Private communcation with Walter Webb, Jarden Applied Materials (2010).

23. Chae HG, Kumar S (2006) Rigid-rod polymeric fibers. *J. Appl. Polym. Sci.* 100:791-802.

24. Yang HH (2007) in *Handbook of Fiber Chemistry*, ed Lewin M (CRC Press, Boca Raton) p. 939.

25. Alexandre M, Dubois P (2000) Polymer-layered silicate nanocomposites: preparation, properties, and uses of a new class of materials. *Mater. Sci. Eng. R. Rep.* 28:1-63.

26. Lee HN, Paeng K, Swallen SF, Ediger MD (2009) Direct measurement of molecular mobility in actively deformed polymer glasses. *Science* 323:231-234.

27. Mauser C, et al. (2008) Anisotropic optical emission of single CdSe/CdS tetrapod heterostructures: Evidence for a wavefunction symmetry breaking. *Phys. Rev. B.* 77:153303.

28. Vanni S, Lagerholm BC, Otey C, Taylor DL, Lanni F (2003) Internet-based image analysis quantifies contractile behavior of individual fibroblasts inside model tissue. *Biophys. J.* 84:2715-2727.

29. Wang N, Ostuni E, Whitesides GM, Ingber DE (2002) Micropatterning tractional forces in living cells. *Cell Motil. Cytoskeleton* 52:97-106.

30. Orendorff CJ, Baxter SC, Goldsmith EC, Murphy CJ (2005) Light scattering from gold nanorods: tracking material deformation. *Nanotechnology* 16:2601-2605.

31. Stone JW, Sisco PN, Goldsmith EC, Baxter SC, Murphy CJ (2007) Using gold nanorods to probe cell-induced collagen deformation. *Nano Lett.* 7:116-119.

32. Li JJ, et al. (2003) Large-scale synthesis of nearly monodisperse CdSe/CdS core/shell nanocrystals using air-stable reagents via successive ion layer adsorption and reaction. *J. Am. Chem. Soc.* 125:12567-12575.

Figure Legends

Fig. 1. Incorporation of CdSe/CdS tetrapods into single polyester fibers. (*A*) The CdSe/CdS tetrapod is a tetrahedrally-symmetric nanocrystal consisting of a zinc-blende CdSe core (red) with four CdS arms (orange). (*B*) Red fluorescence is observed throughout a single polyester fiber incorporated with CdSe/CdS tetrapods. (*C*) SEM images demonstrate that tetrapods, which appear in the higher magnification image as lighter-contrast branched particles, are fully embedded within a single polyester fiber.

Fig. 2. Calibration of the tetrapod stress gauge. (*A*) Fluorescence spectra of tetrapods embedded in a single polyester fiber under extension. A fluorescence red-shift is clearly observed with increasing strain. A spectral shoulder matches that of the tetrapods in solution (blue arrow). (*B*) The change in energy of the tetrapod emission-maximum as a function of extension. Traces of single polyester fibers (dotted lines) reveal varied mechanical behavior, consistent with variations in microstructure domains within and among single fibers. The average (solid line) in the elastic regime is correlated with the known Young's modulus of polyester fiber to calibrate the tetrapod stress gauge. Error bars depict the standard deviation of fiber behavior; fit error is within the data markers. (*C*) Emission-maxima of tetrapods in Nomex® (cyan) and nylon (blue) single fibers as a function of fiber extension (dotted lines) and the corresponding average (solid lines) demonstrate an accurate measure of the Young's modulus of these fibers (black, literature values). The error bars represent the error in calculated modulus due to linear fit.

Fig. 3. Local stresses in a single polyester fiber. (*A*) A spatially resolved profile of the stresses along a fiber with increasing tensile strain. Fluorescence along the same section of fiber is monitored throughout; however, this length increases as the fiber is extended and thus

fluorescence spectra are collected at a greater number of 400 μm spots. 20 data points are collected at 0% extension up to 26 data points at 22.5% extension. (*B*) Area-normalized histograms of the tetrapod emission-maximum along the fiber at increasing fiber extension using data from the stress profile in (*A*), with 0.1 nm bin size. The stress distribution narrows with fiber extension and then widens, indicating that the stresses initially become more homogeneous upon tensile strain, and become increasingly heterogeneous after plastic onset.

Fig. 4. Effects of size and morphology on stress sensing. (*A*) CdSe/CdS tetrapods with shorter (red) and longer (blue) arms both exhibit reduced stress sensitivity in tensile experiments. (*B*) CdSe/CdS quantum dots (pink) show a blue-shift with increasing tensile strain, similar to their behavior under hydrostatic pressure, while CdSe/CdS quantum rods (orange) show no net shift. Both quantum dots and rods do not exhibit a clear identification of sensitivity to anisotropic stress. Error bars in (*A*) and (*B*) represent the standard deviation of single fiber behavior; only the four median plots from each sample are shown for clarity.

Figure 1.

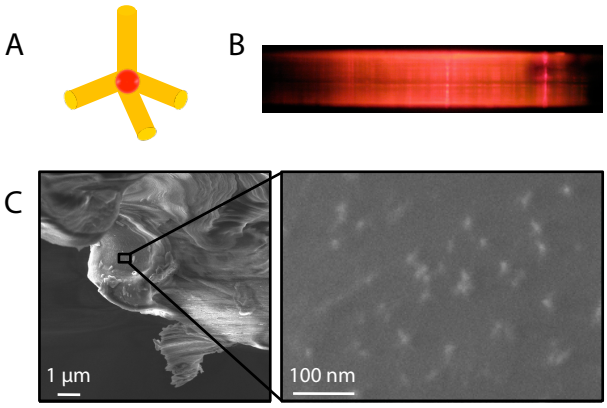

Figure 2.

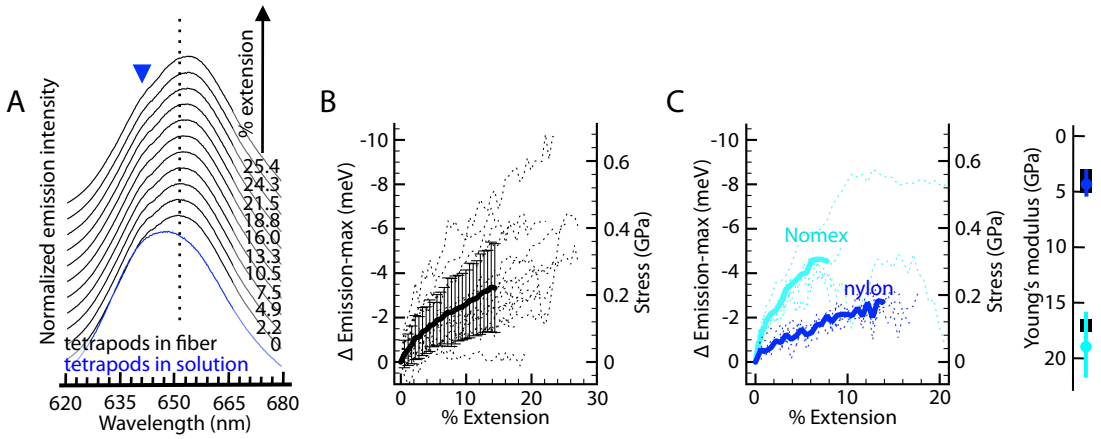
A
Normalized emission intensity
% extension
25.4
24.3
21.5
18.8
16.0
13.3
10.5
7.5
4.9
2.2
0
tetrapods in fiber
tetrapods in solution
620 635 650 665 680
Wavelength (nm)
B
Δ Emission-max (meV)
Stress (GPa)
% Extension
C
Nomex
nylon
Young's modulus (GPa)

Figure 3.

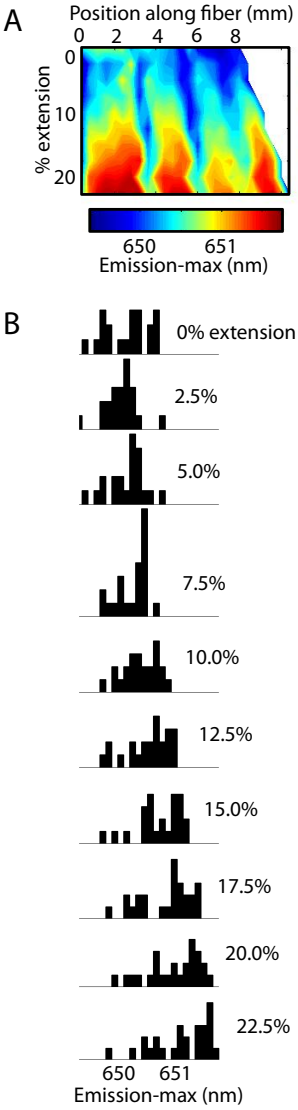
A
Position along fiber (mm)
0 2 4 6 8
0
10
20
% extension
650 651
Emission-max (nm)
B
0% extension
2.5%
5.0%
7.5%
10.0%
12.5%
15.0%
17.5%
20.0%
22.5%
650 651
Emission-max (nm)

Figure 4.

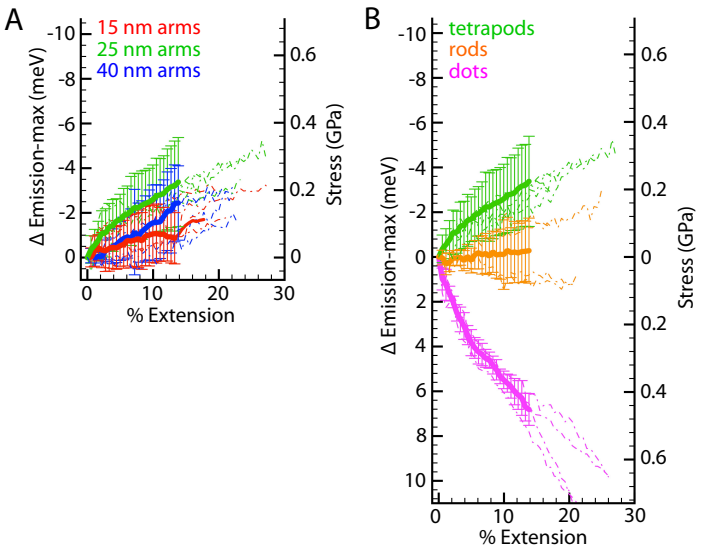
A
15 nm arms
25 nm arms
40 nm arms
Δ Emission-max (meV)
Stress (GPa)
% Extension
B
tetrapods
rods
dots
Δ Emission-max (meV)
Stress (GPa)
% Extension